The conduction gap in double gate bilayer graphene structures

2010 J. Phys.: Condens. Matter 22 115304

(http://iopscience.iop.org/0953-8984/22/11/115304)

IOP Publishing Journal of Physics: Condensed Matter

J. Phys.: Condens. Matter **22** (2010) 115304 (6pp) doi:10.1088/0953-8984/22/11/115304

The conduction gap in double gate bilayer graphene structures

V Hung Nguyen[1,2], A Bournel[1] and P Dollfus[1]

[1] Institut d'Electronique Fondamentale, UMR8622, CNRS, Université Paris Sud, 91405 Orsay, France

[2] Theoretical Department, Institute of Physics, VAST, PO Box 429 Bo Ho, Hanoi 10000, Vietnam

E-mail: viet-hung.nguyen@u-psud.fr

Received 8 December 2009, in final form 18 January 2010
Published 23 February 2010
Online at stacks.iop.org/JPhysCM/22/115304

Abstract

Using the nonequilibrium Green function method, the electrical behavior of a double gate bilayer graphene structure is investigated. Due to energy bandgap opening when potential energies in the layers are different, a clear gap of electrical current is observed. The sensitivity of this phenomenon to device parameters (gate length, temperature) has been considered systematically. It appears that the threshold voltage can be controlled by tuning the gate voltages and/or the Fermi energy. Our obtained results may be useful and provide new suggestions for further experimental investigations.

(Some figures in this article are in colour only in the electronic version)

Graphene and graphene-based nanostructures have become the subject of intensive research in both fundamental and applied physics [1–4]. It results from their unusual electronic properties and their potential for applications in nanoelectronics. A number of unusual transport properties such as finite minimal conductivity [1], unconventional quantum Hall effect [2], Klein paradox [5], etc, have been explored. Additionally, due to carrier mobility as high as 15 000 $cm^2\ V^{-1}\ s^{-1}$ at room temperature [6], graphene is expected to become a basic material for designing high performance devices [7–10]. However, an important drawback of graphene regarding transistor operation is in the lack of energy gap between valence and conduction bands. Therefore, the electrical conduction cannot be fully switched off by tuning the gate voltage, which is necessary for digital electronic applications. As a possibility to overcome this limitation, it was shown that the bandgap can be induced in monolayer graphene (MG) by controlled structural modification of the graphene channel [7], by interaction of the sample with the substrate [11], and/or by patterning it into nanoribbons [12]. More simply, in bilayer graphene (BG) it was demonstrated experimentally that a bandgap up to 250 meV can be generated and controlled by applying an electric field perpendicularly to the sample [13–16]. Motivated by this result, investigations of the transport properties in BG barriers [17, 18], BG-FET [19, 20], and quantum dots [21] have been recently conducted.

In this view, the systematical study of electrical behaviors in BG structures with a gate-induced energy bangap is very timely and desirable for the development of graphene nanoelectronics. Recently, an efficient calculation method based on the nonequilibrium Green function (NEGF) formalism has been developed and was then applied to analyze the electronic transport of charges in single barrier MG [22, 23] and BG [24] structures. Using this method, in this paper we investigate the electrical characteristics of a BG structure when the potential energies in the layers are different. Particularly, we focus on the possibility of obtaining a conduction gap and on its sensitivity to the device parameters.

Bilayer graphene material consists of two A–B-stacked monolayers of graphene as shown schematically in figure 1(a), together with a cross section of the considered structure. The potential energy diagram (just a function of x) is illustrated in figure 1(b). In [25], McCann studied the energy bands of single gate BG structures and showed that the gate-induced potential difference in the layers opens a gap between the conduction and valence bands. He found a roughly linear relationship between the bandgap and the accumulated charge on the bilayer (see equation (5) in [25]). Therefore, the gate can be used to control the charge density and the bandgap (or potential difference) simultaneously. The gate-induced bandgap opening in double gate BG structures has been also demonstrated experimentally [14, 15] and discussed

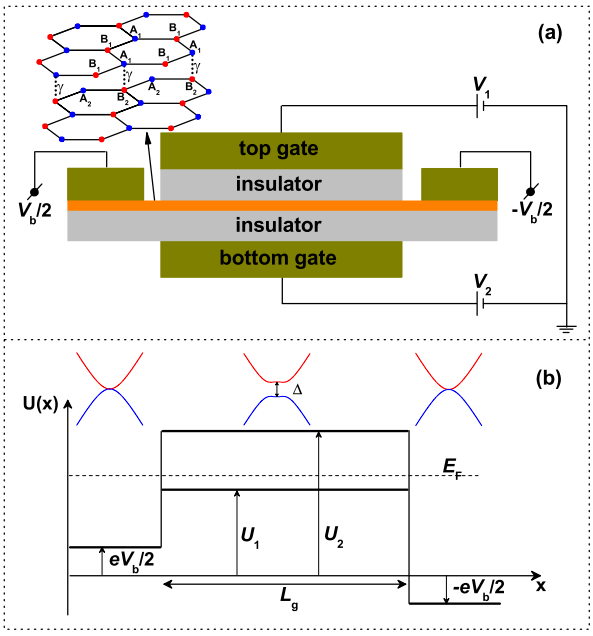

Figure 1. (a) Schema and (b) potential energy diagram of the considered structure.

theoretically, for instance, in [26]. It was shown that the double gated structure can make it possible to control independently the charge density and the bandgap (or potential difference) [14]. As in the experimental setup described in [14], we assume here that the top and bottom gates are used to control the potential energies $U_{1,2}$ in the layers (see in figure 1(b)). The bias voltages $V_b/2$ and $-V_b/2$ are applied to the left and right electrodes, respectively. The Hamiltonian, obtained by expanding the momentum close to the $\boldsymbol{K}$ point [4] in the Brillouin zone, reads

$$H = \begin{pmatrix} v_F\vec{\sigma}\,\vec{p} + U_1 & \tau \\ \tau^\dagger & v_F\vec{\sigma}\,\vec{p} + U_2 \end{pmatrix}, \qquad \tau = \begin{pmatrix} 0 & 0 \\ \gamma & 0 \end{pmatrix} \tag{1}$$

with the Pauli matrices $\vec{\sigma} \equiv (\sigma_x, \sigma_y)$, the 2D-momentum vector $\vec{p} \equiv (p_x, p_y)$, the Fermi velocity of the monolayer modes $v_F \approx 10^6$ m s^{-1}, and the hopping element between A_1 and B_2 sites $\gamma \approx 0.39$ eV.

The Hamiltonian (1) in a new basis $\{|x_n\rangle, |k_y\rangle\}$ [24] is rewritten as

$$\begin{aligned} H_{l,n} &= -\mathrm{i}\Lambda\delta_{n,l-1} + H_l\delta_{n,l} + \mathrm{i}\Lambda\delta_{n,l+1}, \\ H_l &= \begin{pmatrix} U_{1l} + E_y\sigma_y & \tau \\ \tau^\dagger & U_{2l} + E_y\sigma_y \end{pmatrix} \\ \Lambda &= E_0 \begin{pmatrix} \sigma_x & 0 \\ 0 & \sigma_x \end{pmatrix} \end{aligned} \tag{2}$$

where $E_y = \hbar v_F k_y$ and $E_0 = \hbar v_F/2a$ with the transverse momentum k_y ($|k_y\rangle = \mathrm{e}^{\mathrm{i}k_y y}$) and the mesh spacing $a = x_{n+1} - x_n$. Throughout the work, a is chosen to be 0.2 nm, which is proved to be small enough to give accurate results. Using the Hamiltonian (2), the device Green function is defined as

$$G(E) = [E + \mathrm{i}0^+ - H_D - \Sigma_L - \Sigma_R]^{-1} \tag{3}$$

with the device-to-contact coupling self-energy Σ_α calculated from $\Sigma_\alpha = \Lambda g_\alpha \Lambda$ ($\alpha = \mathrm{L}, \mathrm{R}$). The surface Green function

$$g_\alpha = [E + \mathrm{i}0^+ - H_\alpha - \Lambda g_\alpha \Lambda]^{-1} \tag{4}$$

is solved by using the fast iterative scheme described in [27], where H_α is the contact surface Hamiltonian.

The transmission coefficient and the local density of states (LDOS) are defined as

$$\mathcal{T}(E) = \mathrm{Tr}[\Gamma_L G \Gamma_R G^\dagger], \tag{5}$$

$$D(x_n, E) = -\frac{1}{\pi}\mathrm{Im}[G_{n,n}(E)], \tag{6}$$

respectively. The tunneling rate for the left (right) contact is $\Gamma_{L(R)} = \mathrm{i}(\Sigma_{L(R)} - \Sigma^\dagger_{L(R)})$. The current density is then computed from the Landauer formula as

$$J = \frac{2e}{\pi h}\int_{-\infty}^{\infty} \mathrm{d}E\,\mathrm{d}k_y \mathcal{T}(E, k_y)[f_L(E) - f_R(E)] \tag{7}$$

where $f_{L(R)}(E) = 1/[1 + \exp(\frac{E - E_{F_{L(R)}}}{k_b T})]$ is the Fermi distribution function in the left (right) contact with the Fermi level $E_{F_{L(R)}}$.

Using the formalism described above, we now consider the transport properties of the unbiased structure. We plot the map of LDOS in figures 2(a) and (c) and the corresponding transmission coefficient as a function of energy in figures 2(b) and (d) for structures of two different gate lengths. Note that from equation (1), in the limit of infinite (or large) gate length, the spectrum of the BG in the gated region consists of four bands given by $(E - U_m)^2 = \hbar^2 v_F^2 k^2 + \Delta^2/4 + \gamma^2/2 \pm \sqrt{(\gamma^2 + \Delta^2)\hbar^2 v_F^2 k^2 + \gamma^2/4}$ [25] with $U_m = (U_1 + U_2)/2$ and $\Delta = U_2 - U_1$. Therefore, the energy gap between the conduction and valence bands, occurring at $k \neq 0$, is

$$E_g = \frac{\gamma|\Delta|}{\sqrt{\Delta^2 + \gamma^2}}. \tag{8}$$

For strong asymmetry $|\Delta| \gg \gamma$, it saturates at $E_g \approx \gamma$ and for weak asymmetry $|\Delta| \ll \gamma$, we have $E_g \approx |\Delta|$. Accordingly, as seen in figures 2(a) and (c), the maps of LDOS show clearly three energy regions: R_C, R_E, and R_B. The R_C is the classical conduction region, in which the transmission coefficient, in principle, tends to unity when increasing the energy (i.e. thermionic conduction above the barrier). In the R_B-region, some hole bound states appear in the valence band of the barrier, which results in resonant tunneling effects (see in figures 2(b) and (d)). The last one, the R_E-region, is generated when the potential energies in two graphene layers are different, which results in an energy bandgap opening. Therefore, the gated region is occupied fully by evanescent states. Due to the tunneling processes via such evanescent states, the transmission coefficient exhibits an energy gap, which is determined approximately by equation (8) and appears more clearly when the gate length is larger (see in figure 2). The resonant tunneling effects in the R_B-region, which may lead to negative different conductance and oscillation of transconductance, has been investigated carefully

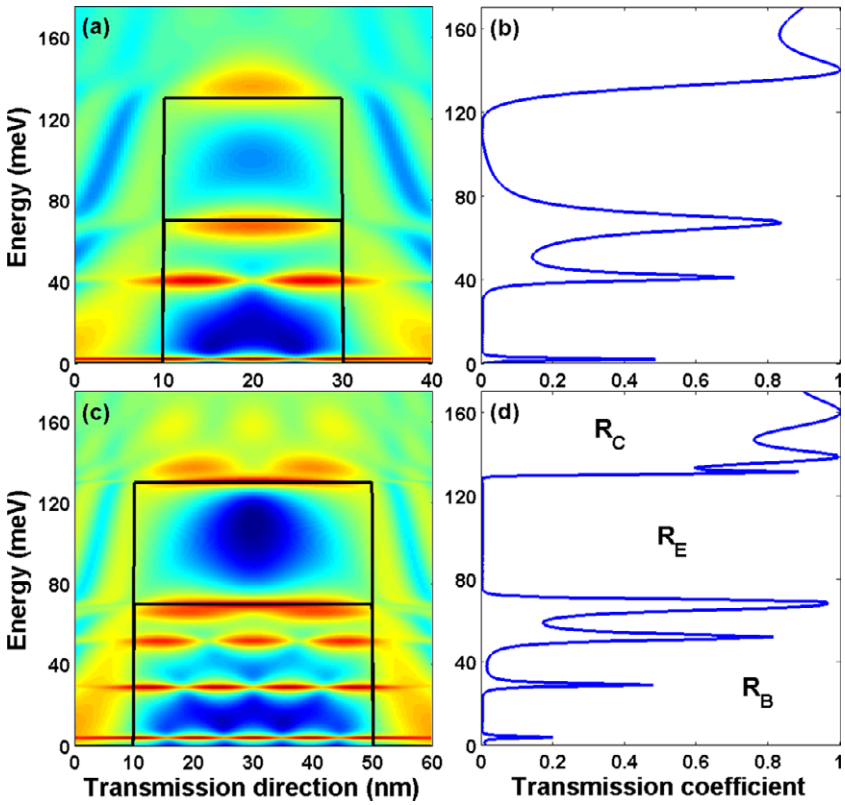

Figure 2. Local density of states and corresponding transmission coefficient for two structures: $L_g = 20$ nm ((a), (b)) and 40 nm ((c), (d)). The black lines in ((a), (c)) indicate the potential profiles in two graphene layers. Everywhere, $E_y = 10$ meV. The structure is unbiased.

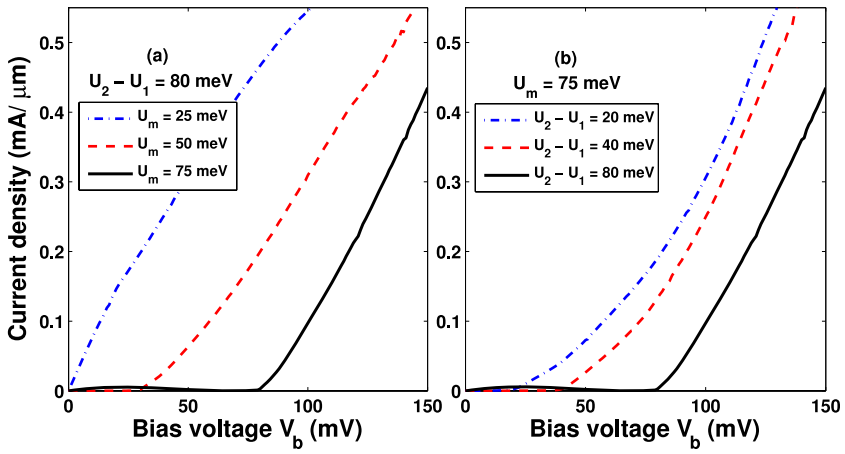

Figure 3. I–V characteristics with different potential energy configurations. Other parameters are $L_g = 40$ nm, $E_F = 75$ meV, and $T = 0$ K.

in [24]. In the current work we mainly focus on the electrical behavior of the structure in the two other regions R_E and R_C.

The feature described above is expected to result in interesting electrical behavior, e.g. the gap of electrical current. For illustration, we plot in figure 3 I–V characteristics at zero temperature for different potential energy configurations. In figure 3(a), while the potential difference $\Delta = 80$ meV is constant, we present the evolution of the I–V curve for different U_m-values. Note that in the case of $U_m = 25$ meV, the Fermi level ($E_F = 75$ meV) is inside the R_C-region and therefore the I–V characteristics are linear at low bias voltages. The situation changes when the Fermi level goes inside the R_E-region as in the two cases of $U_m = 50$ and 75 meV. As shown, it is necessary to apply a finite bias voltage higher than a threshold value V_T to open the channel. This is essentially due to the fact that for a low bias voltage $V_b < V_T$ the whole energy range $[E_F - eV_b/2, E_F + eV_b/2]$ is inside the R_E-region and the channel is thus closed. When the bias voltage is high enough $V_b > V_T$, due to the contribution of carriers of energy beyond the R_E-region, the current takes a significant value. For a given bandgap E_g (or Δ), V_T has its maximum value for $U_m = E_F$ (see in figure 3(a)).

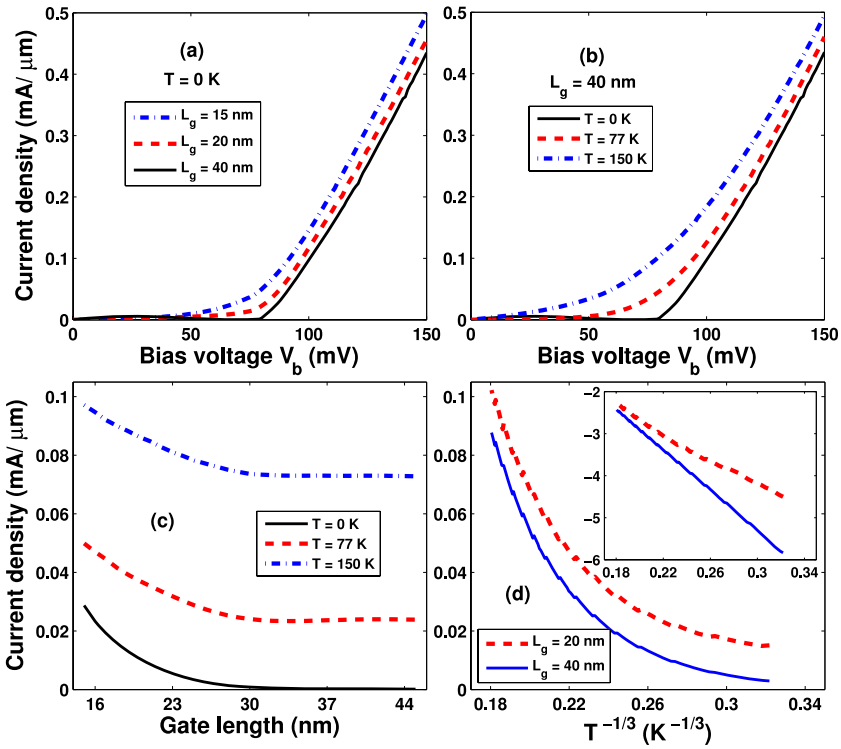

Figure 4. Current density with different gate lengths ((a), (c)) and effects of finite temperature ((b), (d)). The inset of (d) is plotted on a logarithm scale. Other parameters are $E_F = 75$ meV, $U_m = 75$ meV, $U_2 - U_1 = 80$ meV, and for ((c), (d)) $V_b = 70$ mV.

Additionally, the I–V curves are also plotted for different values of Δ in figure 3(b). As discussed above and can be seen in the figures, at zero temperature, the threshold voltage is simply determined as $V_T = (E_g - 2|E_F - U_m|)/e$. For instance, $V_T \approx 28.4$ and 78.4 mV for $U_m = 50$ and 75 meV, respectively, as seen in figure 3(a) or $V_T \approx 19.9$, 39.8 and 78.4 mV for $\Delta = 20$, 40 and 80 meV, respectively, as seen in figure 3(b). Hence, V_T can be modulated by tuning Δ (or E_g), U_m, and/or the Fermi energy E_F (not shown).

The observed features of course are sensitive to other device parameters such as the gate length and the temperature. On the one hand, due to the role of evanescent waves that decay exponentially when increasing the gate length, the energy gap in the R_E-region (shown in figure 2) is smeared when reducing the gate length. On the other hand, the energy range where the carriers can contribute to the current is enlarged when increasing the temperature. As a consequence, smearing effects of the current gap occur when reducing the gate length and/or increasing the temperature as shown in figures 4(a) and (b), respectively. The effects are exhibited more clearly in figure 4(c). At zero temperature, it is shown that the current decays exponentially and tends to zero with respect to the gate length, which is nothing, but the role of tunneling processes via evanescent states. At finite temperature, due to the contributions of carriers of energy beyond the R_E-region, the current tends to a finite value when increasing the gate length. Additionally, we plot the current density as a function of $T^{-1/3}$ in figure 4(d) and on a logarithm scale in the inset. Roughly speaking, its temperature dependence $J(T) \propto \exp[-(T_0/T)^{1/3}]$ is in qualitative agreement with experimental results of [14] where the temperature dependence of resistance at the charge neutrality point has been observed as $R(T) \propto \exp(T_0/T)^{1/3}$. Moreover, consistently with the results presented in figure 4(c), the value of T_0, which can be experimentally measured, decreases when reducing the gate length.

Another way of studying the current gap is to plot the current density versus the potential difference Δ for a fixed bias voltage, as shown in figure 5. In general, it is shown that the current has its maximum value at $\Delta = 0$ and decreases rapidly with increasing Δ. As seen in figures 5(a) and (b), the current peak is defined clearly in the region $|\Delta| < \Delta_T$ where Δ_T is determined from equation (8) with $E_g \equiv E_T$, i.e. $E_T = 2|E_F - U_m| + eV_b$ at zero temperature as mentioned above. For instance, $\Delta_T = 25.1$, 50.4, and 103.5 meV for $V_b = 25$, 50, and 100 mV, respectively, as seen in figure 5(a) or $\Delta_T = 162.5$, 103.4, and 50.4 meV for $U_m = 25$, 50, and 75 meV, respectively, as seen in figure 5(b). Thus, the value of Δ_T also can be modulated by changing E_F (not shown), U_m, and/or V_b. Next, in figure 5(c) we display the current density with different gate lengths. It is shown that, in the case of small gate length, the current exhibits tails with significant values when $|\Delta| > \Delta_T$. This is essentially a consequence of the dependence of evanescent waves (energy gap) on the gate length as presented in figures 2 and 4(a) and (c), e.g. the current gap is smeared when reducing the gate length. Finally, the effects of finite temperature are displayed in figure 5(d). The obtained results show that the current seems to decay exponentially with respect to Δ when the temperature is high enough. It is worth noting that at a moderate temperature of

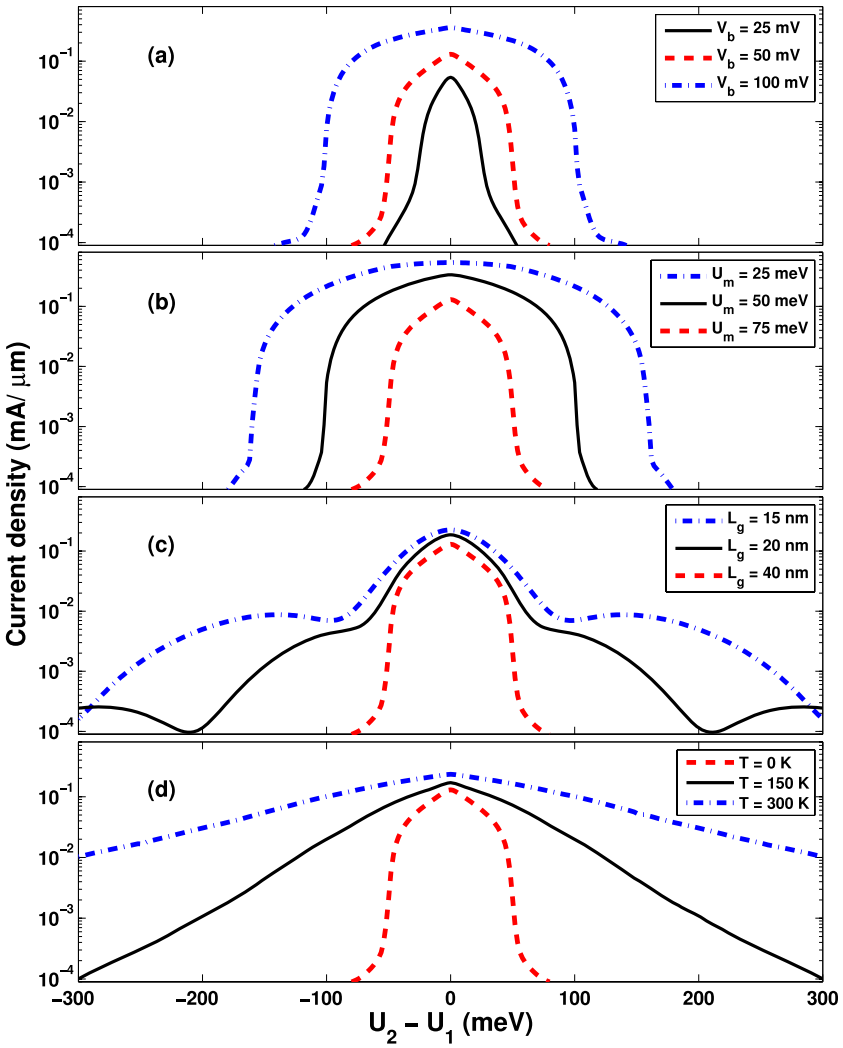

Figure 5. Current density as a function of potential difference $U_2 - U_1$ with different device parameters. Unless otherwise stated, $U_m = 75$ meV, $L_g = 40$ nm, $V_b = 50$ mV, $E_F = 75$ meV, and $T = 0$ K.

150 K, the current decreases by a significant factor of $\propto 10^3$ on changing Δ from 0 to 300 meV ($E_g \approx$ 0–238 meV). However, because of the smearing effect, this factor is reduced when increasing the temperature, e.g. it is about 20–30 at $T = 300$ K as seen in figure 5(d). Recently, it has been suggested that to achieve a sufficiently large I_{on}/I_{off} ratio for circuit applications, other device such as BG tunnel FETs should be designed [28].

In conclusion, by using the NEGF technique, we have considered the electrical behavior of a double gate bilayer graphene structure. As a consequence of energy bandgap opening when the potential energies in the layers, which can be controlled by the gate voltages, are different, the structure exhibits a significant gap of electrical current. The sensitivity of this behavior to all device parameters has been investigated carefully. It is shown that due to the role of tunneling processes via evanescent states the current gap is smeared not only by increasing the temperature but also by decreasing the gate length. A finite threshold voltage can be achieved and controlled by tuning the gate voltages and/or the Fermi energy. These results may be useful and provide new suggestions for further investigations, e.g. in the experimental setup described in [14].

Acknowledgments

This work was partially supported by the European Community through the Network of Excellence NANOSIL and by the French ANR through the project NANOSIM-GRAPHENE. V H Nguyen acknowledges the AUF for financial support. The authors would like to thank Van Lien Nguyen for fruitful discussions.

References

[1] Novoselov K S, Geim A K, Morozov S V, Jiang D, Katsnelson M I, Grigorieva I V, Dubonos S V and Firsov A A 2005 *Nature* **438** 197

[2] Novoselov K S, McCann E, Morozov S V, Fal'ko V I, Katsnelson M I, Zeitler U, Jiang D, Schedin F and Geim A K 2006 *Nat. Phys.* **2** 177

[3] Cresti A, Nemec N, Biel B, Niebler G, Triozon F, Cuniberti G and Roche S 2008 *Nano Res.* **1** 361

[4] Castro Neto A H, Guinea F, Peres N M R, Novoselov K S and Geim A K 2009 *Rev. Mod. Phys.* **81** 109
[5] Katsnelson M I, Novoselov K S and Geim A K 2006 *Nat. Phys.* **2** 620
[6] Geim A K and Novoselov K S 2007 *Nat. Mater.* **6** 183
[7] Echtermeyer T J, Lemme M C, Baus M, Szafranek B N, Geim A K and Kurz H 2008 *IEEE Electron Device Lett.* **29** 952
[8] Sordan R, Traversi F and Russo V 2009 *Appl. Phys. Lett.* **94** 073305
[9] Wang H, Nezich D, Kong J and Palacios T 2009 *IEEE Electron Device Lett.* **30** 547
[10] Zhao P, Chauhan J and Guo J 2009 *Nano Lett.* **9** 684
[11] Zhou S Y, Gweon G-H, Fedorov A V, First P N, de Heer W A, Lee D-H, Guinea F, Castro Neto A H and Lanzara A 2007 *Nat. Mater.* **6** 770
[12] Han M Y, Ozyilmaz B, Zhang Y and Kim P 2007 *Phys. Rev. Lett.* **98** 206805
[13] Castro E V, Novoselov K S, Morozov S V, Peres N M R, dos Santos J M B L, Nilsson J, Guinea F, Geim A K and Castro Neto A H 2007 *Phys. Rev. Lett.* **99** 216802
[14] Oostinga J B, Heersche H B, Liu X, Morpurgo A F and Vandersypen L M K 2008 *Nat. Mater.* **7** 151
[15] Zhang Y, Tang T-T, Girit C, Hao Z, Martin M C, Zettl A, Crommie M F, Shen Y R and Wang F 2009 *Nature* **459** 820
[16] Russo S, Craciun M F, Yamamoto M, Tarucha S and Morpurgo A F 2009 *New J. Phys.* **11** 095018
[17] Nilsson J, Castro Neto A H, Guinea F and Peres N M R 2007 *Phys. Rev.* B **76** 165416
[18] Barbier M, Vasilopoulos P, Peeters F M and Pereira J M Jr 2009 *Phys. Rev.* B **79** 155402
[19] Ouyang Y, Campbell P and Guo J 2008 *Appl. Phys. Lett.* **92** 063120
[20] Fiori G and Iannaccone G 2009 *IEEE Electron Device Lett.* **30** 261
[21] Pereira J M Jr, Vasilopoulos P and Peeters F M 2007 *Nano Lett.* **7** 946
Pereira J M Jr, Peeters F M, Vasilopoulos P, Costa Filho R N and Farias G A 2009 *Phys. Rev.* B **79** 195403
[22] Nam Do V, Hung Nguyen V, Dollfus P and Bournel A 2008 *J. Appl. Phys.* **104** 063708
[23] Nam Do V and Dollfus P 2009 *J. Appl. Phys.* **106** 023719
[24] Hung Nguyen V, Bournel A, Lien Nguyen V and Dollfus P 2009 *Appl. Phys. Lett.* **95** 232115
[25] McCann E 2006 *Phys. Rev.* B **74** 161403(R)
[26] Gava P, Lazzeri M, Saitta A M and Mauri F 2009 *Phys. Rev.* B **79** 165431
[27] Lopez Sancho M P, Lopez Sancho J M and Rubio J 1984 *J. Phys. F: Met. Phys.* **14** 1205
[28] Fiori G and Iannaccone G 2009 *IEEE Electron Device Lett.* **30** 1096